ORIGINAL ARTICLE

Cognitive Control Network Contributions to Memory-Guided Visual Attention

Maya L. Rosen[1], Chantal E. Stern[1,2,3], Samantha W. Michalka[3], Kathryn J. Devaney[1], and David C. Somers[1,2,3]

[1]Department of Psychological and Brain Sciences, [2]Center for Memory and Brain, and [3]Graduate Program for Neuroscience, Boston University, Boston, MA 02215, USA

Address correspondence to David C. Somers, PhD, 2 Cummington Mall, Room 109, Boston, MA 02215, USA. Email: somers@bu.edu

Abstract

Visual attentional capacity is severely limited, but humans excel in familiar visual contexts, in part because long-term memories guide efficient deployment of attention. To investigate the neural substrates that support memory-guided visual attention, we performed a set of functional MRI experiments that contrast long-term, memory-guided visuospatial attention with stimulus-guided visuospatial attention in a change detection task. Whereas the *dorsal attention network* was activated for both forms of attention, the *cognitive control network* (CCN) was preferentially activated during memory-guided attention. Three posterior nodes in the CCN, posterior precuneus, posterior callosal sulcus/mid-cingulate, and lateral intraparietal sulcus exhibited the greatest specificity for memory-guided attention. These 3 regions exhibit functional connectivity at rest, and we propose that they form a subnetwork within the broader CCN. Based on the task activation patterns, we conclude that the nodes of this subnetwork are preferentially recruited for long-term memory guidance of visuospatial attention.

Key words: change detection, functional connectivity, functional MRI, long-term memory, posterior parietal cortex

Introduction

Human visual abilities exceed those of powerful supercomputers, yet our visual performance is profoundly limited by our attentional capacity (e.g., Simons and Chabris 1999). Although humans can attend to multiple objects (e.g., Awh and Pashler 2000; McMains and Somers 2004, 2005; Cave et al. 2010), attentional capacity is limited to approximately 4 objects (Pylyshyn and Storm 1988; Cowan 2001). The paradox of high real-world performance and limited capacity can be reconciled by considering the important role that long-term memory (LTM) plays in guiding visual attention. Prior experience, via either explicit or implicit memory, can accurately direct visual attention and enhance performance (Chun and Jiang 1998, 2003; Henderson and Hollingworth 1999; Moores et al. 2003; Hollingworth 2004, 2005; Summerfield et al. 2006, 2011; Chun and Turk-Browne 2007; Olivers 2011; Patai et al. 2012; Stokes et al. 2012). Despite the functional importance of visual memory-guided attention, its neural mechanisms are understudied compared with other forms of

visual attention [for review, see Hutchinson and Turk-Browne (2012)] and are the focus of the current study.

LTM-guided visual attention should rely on memory retrieval mechanisms and on visual orienting and selection mechanisms. Additionally, we hypothesize that cognitive control mechanisms help to mediate interactions between the attention and memory systems. To investigate this hypothesis, we contrast LTM-guided visual spatial attention with stimulus-guided visuospatial attention in a set of fMRI experiments. Both forms of attention require spatial orienting and selection mechanisms, but differ in memory processing and stimulus processing demands. Prior work has contrasted endogenous or top-down visual attention with exogenous or bottom-up visual attention (e.g., Corbetta and Shulman 2002), focusing on top-down effects driven by the presence of an explicit spatial cue. In contrast, LTM-guided visual attention places different demands on the top-down attentional system and/or may recruit additional brain structures. One prior fMRI study directly contrasted LTM-guided spatial attention

with stimulus-guided attention (Summerfield et al. 2006); this study reported greater left hippocampal activation in the memory-guided condition, but failed to observe differential activation in attentional and control structures. Another LTM-guided attention fMRI study focused on the preparatory activity in spatiotopic parietal cortex and did not include a comparison with stimulus-guided attention (Stokes et al. 2012).

Here, we re-investigate the neural substrates of attentional processes supporting LTM-guided visual spatial attention and focus on 3 prominent brain networks, the *cognitive control network* (CCN), the fronto-parietal *dorsal attention network* (DAN), and the *default mode network* (DMN), including the hippocampus (HC). The DAN, including the intraparietal sulcus/superior parietal lobule/lateral occipital complex (IPS/SPL/LOC), the superior precentral sulcus (sPCS), and the inferior precentral sulcus (iPCS), is typically activated in a broad range of visual attention tasks (e.g., Hagler and Sereno 2006; Konen and Kastner 2008). The DMN, which includes important memory structures such as the HC, parahippocampal cortex (PHC), and posterior cingulate cortex (PCC), is strongly deactivated or suppressed during attentionally demanding tasks (e.g., Raichle et al. 2001). These strongly competitive interactions between attention and memory systems (Buckner et al. 2008; Sestieri et al. 2011; Fox et al. 2005) contrast with the cooperative interactions apparently required for LTM-guided attention (Hutchinson and Turk-Browne 2012). We hypothesize that a third network, the CCN (e.g., Vincent et al. 2008), supports co-operative interactions between explicit LTM and visual spatial attention. This hypothesis is supported by previous work, demonstrating that the CCN is positively correlated with both the DAN and DMN at rest while the correlations between the DAN and DMN are largely negative (Spreng et al. 2013). The CCN supports switching between different mental representations and is a strong candidate to mediate attention–memory interactions (Cole and Schneider 2007; Chiu and Yantis 2009; Spreng et al. 2013). Specifically, medial superior parietal lobe/posterior precuneus (PrC-p) has been implicated in attention switching functions (Shomstein and Yantis 2004, 2006; Chiu and Yantis 2009). Additionally, lateral parietal cortex has been implicated in LTM-retrieval processes related to attention (e.g., Wagner et al. 2005; Cabeza 2008), and several recent studies have sought to functionally parcellate this brain region into different memory and attention subregions (Vilberg and Rugg 2009; Nelson et al. 2010; Sestieri et al. 2010; Hutchinson et al. 2014).

To contrast the cortical networks underlying LTM-guided attention with those underlying visual stimulus-guided attention, we adapted a change detection paradigm (Rensink et al. 1997; Rosen et al. 2014); participants used LTM (LTM-guided) or an exogenous visual cue (STIM-guided) to guide spatial attention to detect scene changes. We performed both whole-brain and region-of-interest (ROI) analyses of fMRI activation patterns during task performance. In a planned analysis, we utilized a cortical surface brain atlas compiled from intrinsic functional connectivity analysis of 1000 brains (Yeo et al. 2011) to define the 3 brain networks and their constituent ROIs. Our results showed that 3 regions located within the posterior CCN were more strongly recruited during LTM-guided attention than STIM-guided attention. This finding was also confirmed in a post hoc analysis suggested by an anonymous reviewer. This post hoc analysis used ROI coordinates derived from 2 alternative network definitions derived from Power et al. (2011) and Yeo et al. (2011). Intrinsic functional connectivity analysis indicated that these 3 regions form a posterior subnetwork within the CCN.

Materials and Methods

Participants

Twenty-three healthy human participants (13 male and 10 female) with normal or corrected-to-normal vision were recruited from Boston University and the greater Boston community. All participants were compensated and gave written informed consent to participate in the study, which was approved by the Institutional Review Board of Boston University. All participants were right-handed and between the ages of 23 and 33.

Visual Stimuli and Experimental Paradigm

Change detection experiments were conducted over 2 sessions: A behavioral training session followed by an fMRI test session. A separate version of the change detection paradigm, with the same images, was used for each session. For training, an extended-exposure, looped version was used to facilitate learning of the scene changes; for the fMRI test session, a brief presentation single-shot version was used to strongly encourage pre-deployment of spatial attention prior to the appearance of the probe stimulus.

Day 1, Training
The initial training session was designed to allow participants to learn a single change in each of 24 scenes (change detection encoding task) that would be used in the LTM-guided attention (LTM-guided) condition on Day 2. Additionally, participants viewed 192 scenes with no changes (man-made/natural judgment task) that would be used in the stimulus-guided attention (STIM-guided) condition during the scan session. Scene stimuli were presented on a Macintosh Macbook Pro laptop computer using the Vision Egg software package (Straw 2008).

Change Detection Encoding Task
Participants were shown 24 scene images in a change detection flicker paradigm (Rensink et al. 1997; Rosen et al. 2014). Each scene was an outdoor scene obtained from Google Images that was altered using Adobe Photoshop (e.g., removed tree, added window, changed color of car, etc.), thus creating 2 versions of each scene (original and altered). On a given trial, a scene appeared on the screen for 1000 ms, followed by a blank screen for 250 ms, and the same scene, containing one change, for another 1000 ms. The original scene and altered scene flickered on and off for 15 s, and participants were instructed to visually search for the change. Detecting changes in novel scenes is attentionally demanding and typically requires several flicker cycles (Rensink et al. 1997). Participants were instructed to click on the scene change using the computer mouse when they detected the change. Following the flicker period was a "reveal period" in which the original and the altered scene alternated without a blank screen for 10 s. In this phase, the altered part of the scene appeared to flicker on and off to attract the participant's attention. The purpose of the reveal period was to ensure that all participants saw all changes and to reinforce the location and identity of the change.

Man-Made/Natural Judgment Encoding Task
Participants also viewed a separate set of 192 scene images for 3000 ms each and made a two-alternative forced choice judgment about whether the scene was mostly natural or mostly man-made. No changes were presented to subjects for this set of images. This exposure served to familiarize participants with the scenes, but not the changes, that would be used in the stimulus-guided (STIM-guided) condition on Day 2.

Day 2, Test

Twenty-four to 48 h after the training day, participants came in for an fMRI scan session. Trials were presented in blocks of 4 different conditions: LTM-guided attention (LTM-guided), exogenous stimulus-guided attention (STIM-guided), uncued scenes (No-Cue), and passive scene viewing (Passive). Each block started with a 1-s block cue period and was followed by six 5.9 s trials, for a total block duration of 36.4 s. A total of 12 counterbalanced blocks were presented per run (4 LTM-guided, 4 STIM-guided, 2 No-Cue, and 2 Passive). Sets of 4 repetition times (TRs; 10.4 s) of blank screen fixation periods were included at the start, halfway point and end of each run. Each run was 7 min 48 s long and 8 runs were performed by each participant.

Practice Session

Participants performed practice trials while in the scanner before the scan session began. In these practice trials, participants maintained fixation at the center of the screen. An image for which they had studied a change the day before appeared on the screen for 3000 ms. Simultaneously, a red and white box outline appeared at the location of the studied change for 1500 ms. Participants were instructed to covertly attend to the location of the box/location of studied change. Then, the image disappeared for 250 ms and flashed up again for 150 ms before being replaced by a blank screen while responses were collected (2500 ms). Participants were instructed to respond whether or not a change occurred at the cued location (50% of trials). These practice trials served 2 purposes. First, participants were trained to maintain fixation at the center of the screen and were given verbal feedback if they made eye movements. Secondly, participants were reminded of the location of the changes in the 24 images that would be used for the LTM-guided condition. This training also ensured that subjects had 3 exposures to the location of the changes in the LTM-guided condition (1 during the initial encoding and 2 during this training). Previous work has suggested that 3 exposures are sufficient for subjects to learn the location and identity of a single change (Rosen et al. 2014).

Scan Session

Participants performed a "single-shot" change detection task under different cueing conditions (Fig. 1). The initial scene appeared for 3000 ms, followed by a blank gray screen for 250 ms, then either the original or altered scene appeared for 150 ms, and finally was replaced by a blank screen for the remainder of each trial (2500 ms) while responses were collected. The single-shot 150-ms probe presentation was chosen to make the attentional selection task difficult, to strongly encourage spatial deployment of attention prior to appearance of the probe, and to prevent subjects from overtly or covertly moving their attentional foci once the probe appeared. The initial image did not provide any information regarding whether a change would occur on that trial. On 50% of the trials, the probe image was different from the initial image (change), and on 50% of trials it was identical to the image presented initially (no-change). Participants made a judgment about whether a change occurred in the probe image compared with the original image. Due to the short duration of the probe stimulus in the change detection task, participants were required to accurately direct spatial attention to detect the image change. In all conditions, participants were instructed to fixate at the center fixation point and direct their attention covertly to the cued location in the scene. In the *LTM-guided attention condition* (*LTM-guided*; Fig. 1A), participants viewed one of the 24 images for which they studied changes the prior day. There was no explicit cue on the images. Participants used memory to direct their attention to the spatial location of the studied change. Image changes occurred on 50% of the trials and only occurred at the studied location. In the *stimulus-guided attention condition* (*STIM-guided*; Fig. 1B), participants viewed one of the 192 scenes that they had studied without image changes the prior day with the addition of an explicit cue. The cue was a set of nested red and white square outlines (~1.3 × 1.3 degrees of visual angle) centered around the location of the potential scene change for 1500 ms at the start of the 3000-ms static image phase. Image changes occurred on 50% of the trials, and only occurred at the cued location. In the *no-cue condition* (No-Cue), participants viewed novel images that had not previously been studied and no cue was provided.
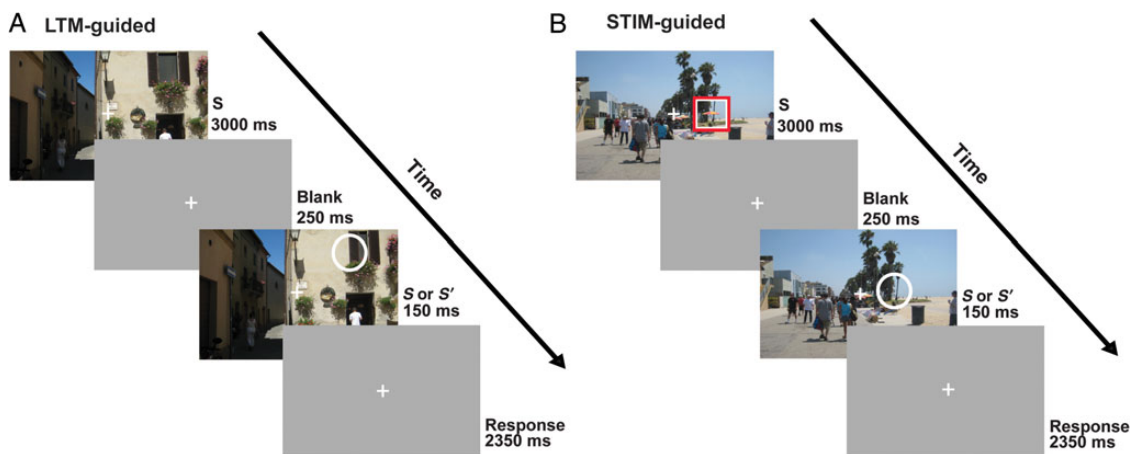

Figure 1. One-shot change detection paradigms. A scene (S) was presented for 3000 ms, followed by a blank screen (250 ms), a very brief presentation (150 ms) of either an identical or altered image (S or S′), and another blank screen (2500 ms). Participants held central fixation while trying to detect whether or not a single change occurred in the scene. (A) LTM-guided condition: Participants viewed scenes for which they had previously learned the location of changes. Participants were instructed to covertly direct attention to the remembered location of the potential change; no explicit spatial cue was provided. (B) STIM-guided condition: Participants viewed scenes that they had previously studied without exposure to scene changes. A red and white square explicitly cued the location of the potential scene change, and then disappeared prior to the image change. Note that the white circle was used in this figure for illustration purposes to highlight the scene change, but no such stimulus appeared on the images.

Participants were instructed to attend to the entire scene and do their best at detecting changes. The condition was included as a behavioral control to demonstrate the impact of LTM-based and stimulus-based cues on behavioral performance. Because this condition had much greater task difficulty, many fewer detected targets, and a greater chance that subjects might incidentally encode the novel scenes and locations of any detected targets, we did not include it as a baseline fMRI condition or in the imaging data analysis (but it was included as a regressor in the model).

In the *passive condition (Passive)*, participants were instructed to fixate as in all other conditions and simply make a random button press whenever the scene appeared for a second time.

Trials were presented in blocks of 6, with each block preceded by a cue word on the screen to indicate the block condition: "memory" for LTM-guided, "box" for STIM-guided, "active" for No-Cue, and "passive" for Passive. A total of 408 images were divided into lists of 24 scenes. Scene images used for each condition were counterbalanced across participants such that each list of 24 was presented in each of the 4 conditions (LTM-guided, STIM-guided, No-Cue, and Passive) across the set of participants and each participant viewed all images. The 24 scenes used in the LTM-guided condition for each participant were repeated once per run (8 times total). All other images were only presented once for each participant.

MR Data Acquisition

Functional MRI data were acquired using a 3-T Siemens TIM Trio MR imager located at the Center for Brain Science at Harvard University in Cambridge, Massachusetts. All data were acquired using a 32-channel head coil. Functional scans were acquired using T_2*-weighted, gradient-echo, echo-planar images [TR = 2.6 s, echo time (TE) = 30 ms; voxel size $3.1 \times 3.1 \times 3.0$ mm] and were collected from 42 slices with no skip, with full brain coverage. Each subject participated in 8 functional scans (each 180 TRs; 7 min 48 s duration) in one scan session. Functional data were aligned with high-resolution ($1.0 \times 1.0 \times 1.3$ mm) T_1-weighted images. For 15 participants, the high-resolution structural images were acquired at the same facility; for 8 participants, they were acquired on an identical scanner and coil at the Martinos Center for Biomedical Imaging at Massachusetts General Hospital in Charlestown, Massachusetts. All high-resolution structural images were used to create a computerized reconstruction of each cerebral cortical hemisphere. Thirteen of the 23 participants returned to undergo a resting-state scan (TR = 2.6 s, TE = 30 ms; voxel size $3.1 \times 3.1 \times 3.0$ mm, 42 slices, no skip). During this scan, they were instructed to fixate at a center fixation cross and otherwise allow their mind to wander. Participants underwent between 6 and 12 min of resting-state scanning.

MR Data Analysis

For each participant, the cortical surface of each hemisphere was computationally reconstructed from the high-resolution anatomical volume using the FreeSurfer software (Dale et al. 1999; Fischl, Sereno, and Dale 1999; Fischl, Sereno, Tootell, et al. 1999; Fischl 2012). Both fMRI task data and fMRI resting-state data were analyzed using the Freesurfer 5.1.0 software package (Charlestown, Boston, MA, USA). For functional data, intensity normalization and motion correction were performed before signal averaging was performed. We analyzed data in 2 ways: first, using a random-effects model, group average data were projected onto the cortical surface of the Freesurfer average (fsaverage) brain (Dale et al. 1999); secondly, by defining multiple ROIs for

each of 3 brain networks (CCN, DMN, and DAN) in each participant. These regions were taken from a publicly available atlas that was originally defined using cluster-based intrinsic functional connectivity analysis of 1000 brains (Yeo et al. 2011, see below for details). Whole-cortex and ROI analyses were performed using a general linear model (GLM) with regressors that matched the time course of all task conditions (LTM-guided, STIM-guided, No Cue, Passive, and Fixation). Resting-state data were analyzed using the cortical ROIs that showed greater activation for LTM-guided attention than STIM-guided attention as seed regions.

Whole-Brain Cortical Surface Analysis

Single participant fMRI data were registered to an average cortical surface space (Freesurfer "fsaverage" brain) using the boundary of the gray matter and white matter. Analyses were performed separately in each hemisphere on the average cortical surface, and data were analyzed for each vertex using a GLM with each condition as a predictor (i.e., one for LTM-guided, STIM-guided, No-Cue, and Passive). Three motion correction regressors were included in the model. The BOLD signal was modeled as a linear, time-invariant system with gamma response function assumed for each condition with a delay $\delta = 2.25$ and a delay time constant $\tau = 1.25$. An estimated response was generated by convolving the response function with the block length (i.e., the time in each condition) and minimizing the residual error (FS-FAST, Cortech). Random-effects group analyses were performed using surface-based averaging techniques (Fischl, Sereno, Tootell et al. 1999). A t-test was performed for each vertex to compare differences in activation between conditions. The significance of these activation differences was projected onto the surface of the Freesurfer "fsaverage" brain.

To correct for multiple comparisons, we employed FS-FAST to perform Monte Carlo simulations of a smoothed null hypothesis data set to establish cluster-wise thresholds for the population maps (Forman et al. 1995). The Monte Carlo simulation generated random volumes of normally distributed values that were then smoothed by a 6-mm smoothing kernel. Clusters were defined as areas of contiguous vertices with significant values below a threshold of $P < 0.01$. Ten thousand iterations of this simulation established a cluster-size threshold of 140 mm^2 for LTM-guided versus STIM-guided contrast. Results are presented in Table 1.

ROI Analysis Within the CCN, DAN, and DMN

We examined whether 3 previously defined cortical networks would be differentially activated in LTM- and STIM-guided attentional conditions: the DAN or task-positive network (Raichle et al. 2001; Corbetta and Shulman 2002), which is involved in top-down endogenous attention, the DMN or task-negative network (Raichle et al. 2001; Buckner and Vincent 2007; Buckner et al. 2008; Vincent et al. 2008), which is recruited in retrieval of LTM, and a third network, the CCN (Vincent et al. 2008), some nodes of which lie adjacent to the nodes of the DMN and/or the DAN. We performed both ROI-based analysis and whole-cortex GLM analysis to contrast the blood oxygen-level-dependent (BOLD) activation in the LTM-guided and STIM-guided conditions. In the ROI analysis, each condition was contrasted with a passive viewing condition to quantify the patterns of activation produced by both forms of attention. Our ROI definitions for the CCN, DAN, and DMN were obtained from the Yeo–Krienen–Buckner cortical network atlas, which was constructed from cluster-

Table 1 Significant areas of activation in the contrast of LTM-guided versus STIM-guided attention conditions

Anatomical region	Hemisphere	x	y	z	Size (mm^2)	t-value
LTM-guided > STIM-guided attention						
Posterior	L	−5.8	−64.5	30.7	1107.61	7.755
Precuneus	R	12.7	−64.2	38.6	774.24	7.15
Mid-cingulate/callosal sulcus	L	−4	−22.3	31	794.16	7.518
	R	5.3	−25.7	29.5	481.18	6.939
Anterior dorsal lateral prefrontal cortex	L	−22.3	43.9	27.7	2060.02	5.975
	L	−39.7	19.8	39.7	173.09	3.829
	R	33.7	48.1	5	1490.59	6.688
AnG/latIPS	L	−48.6	−58.9	38.2	1195.22	5.751
	R	45.5	−56.9	43.2	751.61	5.757
Anterior cingulate cortex	R	12.7	36.4	21.8	253.91	5.114
Cuneus	R	7.2	−74.8	30	330.09	4.807
STIM-guided > LTM-guided attention						
Ventral temporal	L	−46.2	−60.8	−2	10937.29	8.905
Cortex/LOC/IPS/supramarginal gyrus	L	−22.6	−15.3	−22.4	142.09	4.999
	L	−52.7	−27.2	32.7	634.03	5.23
	R	28.9	−67.8	−5.6	14690.27	11.246
sPCS	L	−35.8	−5.8	43.3	525.42	7.007
	R	31.6	−7.5	46.2	916.79	5.989
iPCS	L	−39.9	11.7	20.3	737.76	5.371
	R	45	5.2	26.3	1035.83	5.326
Anterior superior temporal sulcus	R	48	−13.6	−10.6	249.47	5.18
Insula	L	36.5	−4.2	7.3	140.28	5.149
	R	37.8	−1.6	1.5	152.49	4.283
Anterior inferior frontal	L	−40.9	27.6	2	153.97	3.425
Sulcus/gyrus	R	45.6	31.2	5.7	164.18	4.661
Lateral orbitofrontal cortex	R	33.3	30.5	−10.8	311.81	4.589
PrC-a/posterior cingulate sulcus	L	−15.3	−15.8	38.3	153.55	3.702
Parietal occipital sulcus/calcarine sulcus	R	21.8	−50.6	7.8	175.41	3.599

Note: MNI coordinates reflect the peak of each cluster, not the centroid.

based analysis of intrinsic functional connectivity of 1000 brains (Yeo et al. 2011). Our analysis employed 3 of the 7 Yeo–Krienen–Buckner networks (CCN, DAN, and DMN). Each subregion of each of these networks was mapped from a predefined label on the Freesurfer "fsaverage" brain onto the appropriate cortical hemisphere of each participant to define each ROI. The CCN is made up of posterior cortical regions including lateral IPS (latIPS), PrC-p, posterior callosal sulcus (CaS-p)/mid-cingulate, and posterior lateral temporal cortex (LTC-p), and anterior cortical regions within the prefrontal cortex, including dorsolateral prefrontal cortex (dlPFC), posterior dorsomedial prefrontal cortex (dmPFC-p), and posterior ventrolateral prefrontal cortex (vlPFC-p). We note that the latIPS ROI does not include the fundus of IPS, but rather incorporates the more ventral aspect of the lateral bank of IPS as well as the dorsal most portion of the angular gyrus (AnG). The DAN includes a region running from the IPS/SPL through lateral occipito-temporal cortex (IPS/SPL/LOTC), as well as sPCS and iPCS. The DMN includes AnG, PCC/anterior precuneus (PrC-a), anterior lateral temporal cortex (LTC-a), anterior dorsal medial prefrontal cortex (dmPFC-a), anterior vlPFC (vlPFC-a), and PHC. To facilitate comparison with earlier work (Summerfield et al. 2006; Stokes et al. 2012), we also included an anatomically defined hippocampal ROI (see below). Percent signal change was extracted for each condition (LTM-guided and STIM-guided) compared with Passive viewing of the stimuli, and averaged across blocks and runs to construct time course data for all vertices/voxels within each of the 17 ROIs (16 cortical ROIs and 1 hippocampal ROI) per hemisphere for each individual

subject (Figs 3 and 4). A separate three-way (ROI × Condition × Hemisphere) analysis of variance (ANOVA) was then performed for each network (DAN, CCN, and DMN).

Hippocampal ROI Analysis

The HC is known to be involved in LTM encoding and retrieval, and the left HC has been shown to be more activated for LTM-guided attention compared with visual stimulus-guided attention when participants search for a target in a visual scene (Summerfield et al. 2006). Therefore, we identified the left and right hippocampi of each individual participant using Freesurfer's automatic parcellation methods (Fischl et al. 2002). The hippocampal ROIs included the entire anterior–posterior extent of the HC. We then performed an ROI analysis in volume space to calculate the percent signal change for each condition (STIM-guided and LTM-guided) compared with passive viewing. Because of the strong functional and anatomical connections between the HC and the DMN (Vincent et al. 2006; Greicius et al. 2009), we discuss the results from the hippocampal ROI analysis with the DMN results.

ROI Analysis Using Alternative Network ROIs

On the advice of an anonymous reviewer, we performed post hoc analysis of our results using ROIs derived from 2 alternative network definitions that also derive from resting-state functional connectivity, that is, the Power et al. (2011) study and the

Yeo et al. (2011) 17-network parcellation. Both analyses identify a network comprised of the mid-cingulate/CaS-p and the PrC-p/posterior medial parietal cortex. Whereas Yeo and colleagues do not comment on the possible functionality of this network, Power and colleagues performed a meta-analysis of prior work and found evidence that this subnetwork, in conjunction with a small region in the lateral parietal cortex, might support some form of memory retrieval processes. The PrC-p and CaS-p/mid-cingulate coordinates were taken from Power et al. (2011), and coordinates for the lateral parietal region (latIPS) were taken from a paper cited by Power [posterior IPL in Nelson et al. (2010)] and Power (personal communication). We performed ROI analysis on the Montreal Neurological Institute (MNI) coordinates, dilated 8 mm, of these 3 regions. We also performed a subsequent analysis using ROIs from the Yeo et al. 17-network parcellation. In the 17-network parcellation, the 2 medial regions, the PrC-p and the CaS-p/mid-cingulate break off into a subnetwork [gray-blue network in Yeo et al. (2011)]. On the lateral surface, the most lateral portion of the IPS (latIPS) forms into a subnetwork including the superior lateral prefrontal cortex and frontal pole [mauve network in Yeo et al. (2011)]. To investigate the more specific parcellation of the posterior nodes of the CCN, we used the 17-network parcellation to define the 2 medial regions (PrC-p and CaS-p) and the latIPS, and conduct ROI analyses.

Intrinsic Functional Connectivity Analysis

Previous work has found that the CCN is positively correlated at rest with the DAN and DMN (Spreng et al., 2013). Here, we sought to investigate the specific pattern of intrinsic functional connectivity of the 3 nodes of the CCN that were more strongly recruited during LTM-guided attention than STIM-guided attention. All intrinsic connectivity analyses were performed within the hemisphere. Data from resting-state scans were processed in Matlab. Twelve motion regressors (6 motion parameters from Freesurfer and their 6 temporal derivatives) were included in the regression analysis. Nuisance regressors for the white matter, the ventricular cerebrospinal fluid, and the global mean waveform were included in the analysis along with the motion regressors (van Dijk et al. 2010). Framewise displacement was calculated by taking the sum of the absolute value of 6 motion parameters. A threshold of 0.5 mm was set to exclude time points with excessive motion. Runs with >10% of time points removed due to excessive motion were removed from further analyses. High motion time points were temporarily replaced using linear interpolation to avoid artifact spread during band-pass filtering (Power et al. 2012, 2013; Carp 2013). Data were band-pass filtered to extract frequencies between 0.01 and 0.08 Hz, and then high motion time points were removed. We defined 3 seeds (PrC-p, latIPS, and CaS-p) constrained by significant activation ($P < 0.01$) for LTM compared with passive viewing during the task in the group average. A time course was then averaged across vertices for each ROI for each hemisphere. A correlation was then computed between each seed and every vertex in the brain. To correct for multiple comparisons, we again employed FS-FAST to perform Monte Carlo simulations of a smoothed null hypothesis dataset to establish cluster-wise thresholds for the population maps (Forman et al. 1995), as we did for the GLM analysis. The Monte Carlo simulation generated random volumes of normally distributed values that were then smoothed by a 6-mm smoothing kernel. Clusters were defined as areas of contiguous vertices with significance values below a threshold of $P < 0.00833$ (correction for 6 comparisons) and a significant cluster threshold size of 164 mm^2 was established.

Results

Behavioral Results

Participants performed well in the challenging one-shot change detection task for the memory-guided attention (LTM-guided) and visual stimulus-guided (STIM-guided) conditions. Behavioral data are reported for 21 of 23 participants; due to technical difficulties, behavioral data are not available for 2 participants. Change detection performance was not different between the memory-guided (LTM-guided d': 2.64 ± 0.14) and explicit cue (STIM-guided d': 2.45 ± 0.09) conditions ($t_{(20)} = 1.43$ $P = 0.17$). Performance in both conditions was significantly greater than in the No-Cue condition ($d' = 0.94 \pm 0.09$ correct; $P < 0.0001$, Holm–Bonferroni corrected). This demonstrates that both forms of cueing have a substantial impact on performance, and that participants performed at least as well in the LTM-guided condition as in the STIM-guided condition. Because the STIM-guided condition explicitly cued the location of the potential change, these behavioral data also confirm that participants had learned the locations of the changes in the LTM-guided condition images, which did not contain an explicit cue. Additionally, a one-factor ANOVA demonstrated that d' performance did not change over the course of the experiment in the LTM-guided condition ($F_{7,105} = 1.175$, $P = 0.32$), suggesting that subjects had fully encoded the locations of the changes in the LTM-guided condition and were not doing any additional learning over the course of the experiment. Furthermore, there was no difference in reaction time between the STIM-guided and LTM-guided conditions [STIM-guided RT: 1.02 ± 0.05 s and LTM-guided 1.02 ± 0.05 s, $t_{(20)} = 0.1$, $P = 0.92$]. Note that images and changes were counterbalanced across participants (e.g., one participant's LTM-guided images were another participant's STIM-guided images, No-Cue, or Passive images), and thus performance differences between conditions cannot be attributed to the images or changes themselves.

Eye Movements

Participants were instructed to maintain central fixation throughout the experiment during fMRI scanning. Eye position was monitored via a video camera for all subjects and eye movements in excess of 2 degrees of visual angle were recorded. For 3 participants (2 male and 1 female), one run was excluded from fMRI analysis due to excessive (>5% of trials) eye movements during that run. Otherwise, participants overall maintained fixation on 99.0% of trials (STIM-guided: 98.3% and LTM-guided: 99.3%; No-Cue = 99.1%; Passive = 99.2%).

fMRI Results

We performed both whole-cortex surface-based analysis and ROI-based analysis to contrast the BOLD activation in the 2 behaviorally matched conditions, LTM-guided and STIM-guided, to determine which cortical areas are differentially recruited for memory-guided attention and stimulus-guided attention. The ROI analysis includes both a planned comparison across 3 cortical networks (cognitive control, dorsal attention, and default mode) and a post hoc analysis of subnetworks suggested during the review process. The non-task "Passive" condition, which includes stimulus presentation and a button press, served as the baseline condition.

Whole-Cortex Surface-Based Analyses

As an initial step, we performed whole-cortex GLM analysis (Fig. 2). This analysis (LTM-guided > STIM-guided) demonstrated
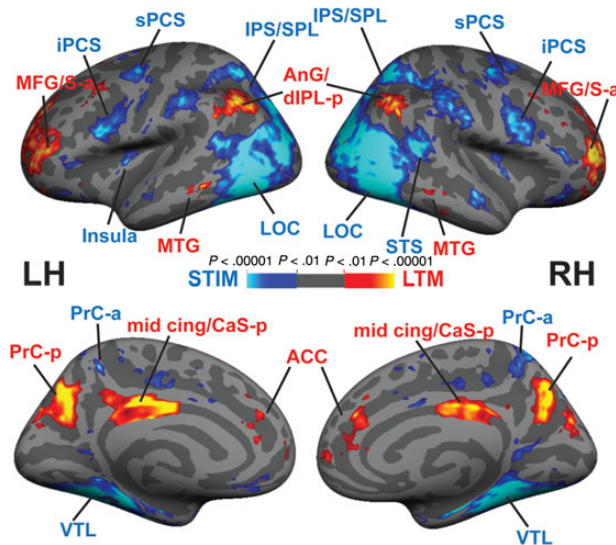
Figure 2. LTM-guided attention versus stimulus-guided attention: a whole-cortex surface-based GLM analysis averaged over all participants ($n = 23$) shows areas that respond differentially to LTM-guided versus stimulus-guided attention. Hot colors represent LTM-guided > STIM-guided and cool colors represent STIM-guided > LTM-guided. See Table 1 for details.

that memory-guided attention differentially activated bilateral regions in PrC-p, CaS-p/mid-cingulate, anterior dlPFC (dlPFC-a), latIPS/AnG, right anterior cingulate (ACC), and right cuneus (Cun; Table 1). However, 3 areas identified in this contrast (LTM-guided > STIM-guided), bilateral dlPFC-a, right ACC, and right Cun actually reflect strong deactivation in those vertices in the STIM-guided condition, while no activation is apparent in those vertices for the LTM-guided condition. Therefore, 3 key bilateral regions demonstrated activation for the LTM-guided spatial attention condition: PrC-p, CaS-p/mid-cingulate, and latIPS/AnG.

The reverse contrast (STIM-guided > LTM-guided) revealed greater bilateral activation in several nodes of the DAN: sPCS, iPCS, and IPS/lateral SPL/LOC (IPS/SPL/LOC; Table 1). Bilateral activation was also observed in the mid insula and anterior inferior frontal sulcus/gyrus, and anterior superior temporal sulcus (STS-a). Unilateral activation was observed in right lateral orbitofrontal cortex, and left posterior cingulate cortex/PrC-a (Table 1).

Network ROI Analysis I—Yeo 7-Network Parcellation

To quantify the patterns of activation produced by both forms of attention, we contrasted the LTM-guided and STIM-guided conditions with a passive viewing non-task condition and performed ROI-based analysis. Our primary interests were in the *cognitive control, dorsal attention*, and *default mode networks* (CCN, DAN, and DMN, respectively). To identify ROIs, we employed an atlas constructed from cluster-based analysis of intrinsic functional connectivity of 1000 brains (Yeo et al. 2011, 7-network parcellation). This atlas contains several subregions within each of the 3 networks (CCN, DAN, and DMN). We mapped these ROIs onto the brains of each subject and extracted percent signal change for each region.

Cognitive Control Network

Nodes of the CCN were activated by both the STIM-guided and LTM-guided conditions relative to passive viewing (Fig. 3A,B and Table 2). A repeated-measures Hemisphere × ROI × Condition ANOVA was performed, and all statistics are lower-bound

corrected (Mauchly's test for sphericity was not met for any of the main effects or interactions; $P < 0.001$). This ANOVA revealed a main effect of Condition such that there was significantly greater activation in the CCN in the LTM-guided condition compared with the STIM-guided condition ($F_{1,22} = 5.29$, $P = 0.031$). The ANOVA also revealed a significant main effect of ROI ($F_{1,22} = 14.05$, $P = 0.001$). There was no main effect of Hemisphere, no interaction for Hemisphere × Condition or Hemisphere × ROI, and no three-way Hemisphere × ROI × Condition interaction ($F_{1,22} = 3.90$, $P = 0.06$; $F_{1,22} = 2.01$, $P = 0.170$; $F_{1,22} = 0.229$, $P = 0.637$; $F_{1,22} = 1.726$, $P = 0.202$, respectively); therefore, we combine data across hemispheres in subsequent analyses.

There was also a significant ROI × Condition interaction ($F_{1,22} = 21.00$, $P < 0.001$). A more in-depth look revealed that this interaction was driven specifically by 2 posterior medial ROIs within the CCN, PrC-p, and CaS-p/mid-cingulate. These regions were also found to be significantly more activated in the LTM-guided condition compared with the STIM-guided condition in the whole-cortex analysis (see above). Percent signal change is presented in Table 2 for all ROIs. Post hoc paired t-tests (Holm–Bonferroni corrected for 34 total ROIs) revealed significantly greater activation for LTM-guided versus STIM-guided in the PrC-p and CaS-p (both $P < 0.001$). latIPS exhibited a similar but weaker activation pattern that did not survive statistical correction for the multiple ROIs; no other CCN areas exhibited significant activation differences between LTM-guided and STIM-guided conditions (Table 2). These findings, taken together with the whole-cortex analysis, demonstrate that the 2 medial posterior nodes of the CCN, PrC-p, and CaS-p make significant contributions to LTM-guided attention.

The maps of the group-level averages for both LTM-guided and STIM-guided compared with passive viewing (Fig. 3C–F) reveal that the activation differences within the PrC-p and CaS-p are precisely captured within the ROIs defined by the Yeo–Krienen–Buckner atlas. Although regions abutting the PrC-p are activated in the STIM-guided condition, PrC-p is essentially devoid of significantly activated vertices in the STIM-guided condition. In contrast, nearly all of PrC-p is significantly activated in the LTM-guided condition. CaS-p is activated (relative to passive viewing) in both the STIM-guided and LTM-guided conditions, but the relative increase in activation for the LTM-guided condition (vs. STIM-guided) can be seen to be restricted to the boundaries of the ROI (Fig. 3C,D). These results also help to functionally validate these CCN ROI definitions of the Yeo–Krienen–Buckner atlas.

The results for latIPS in the ROI analysis are more ambiguous than in the whole-cortex analysis (Fig. 2). LTM-guided attention appears to drive posterior portions of the bilateral latIPS ROIs, whereas the STIM-guided condition fails to drive any portion of the ROIs (Fig. 3E,F); however, the anterior portion of the latIPS ROI is not activated in either condition. A closer analysis reveals a shift in the location of the latIPS peak between the LTM-guided versus STIM-guided contrast (Table 2, shown on the whole cortex; Fig. 2) and the LTM-guided versus baseline contrast (shown on the ROIs; Fig. 3E,F) of 16.7 and 11.6 mm ventrolaterally, in the left (LH) and right hemispheres (RH), respectively. The peak shift reflects the fact that a deactivated DMN region, AnG, lies adjacent to the activated latIPS region, and that the DMN border region is more deactivated during the STIM-guided condition (see Discussion).

Dorsal Attention Network

As expected, the DAN was activated by both the STIM-guided and LTM-guided conditions compared with passive viewing
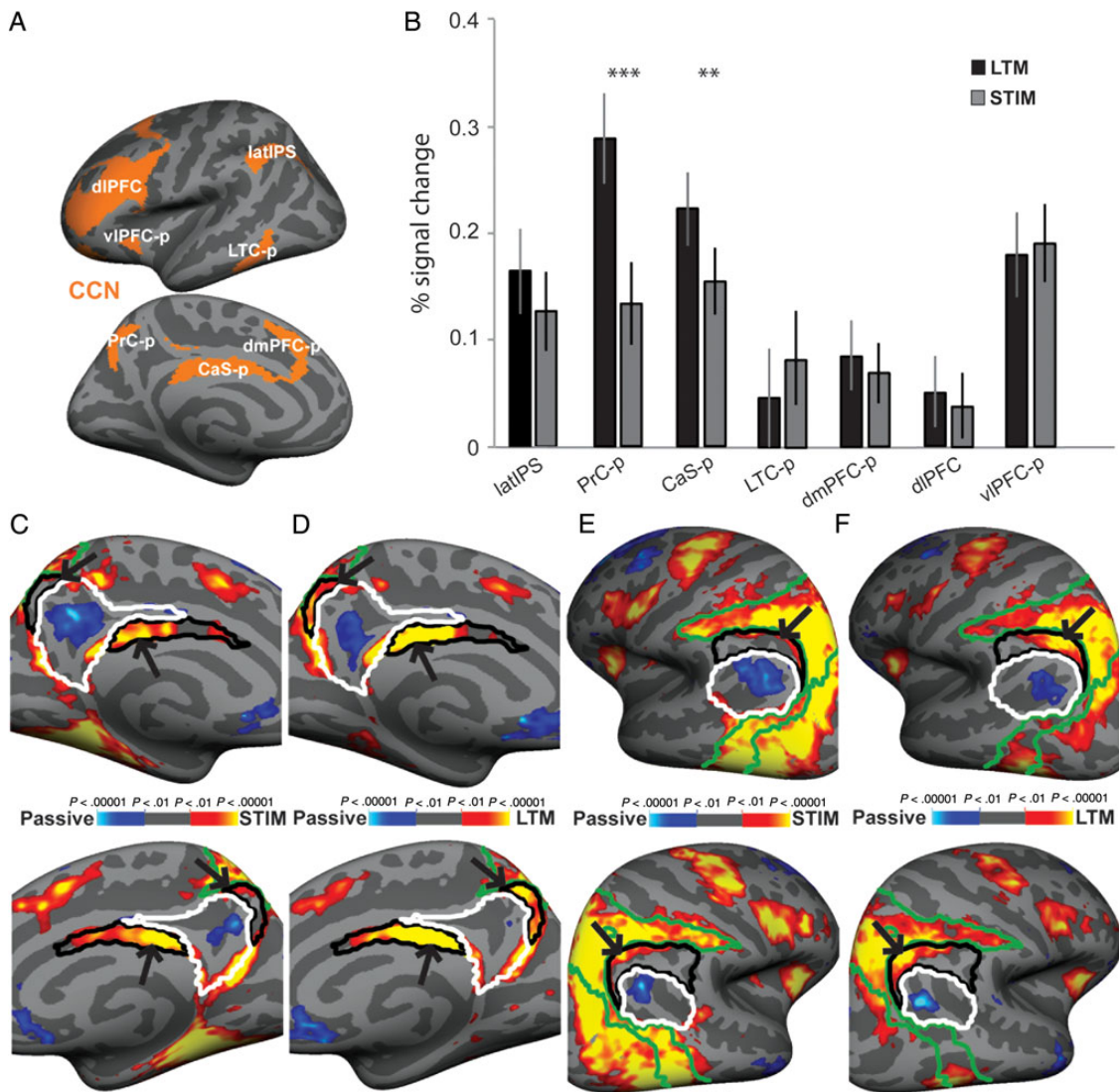
Figure 3. ROI analysis for the CCN: (A) ROIs were obtained from an intrinsic functional connectivity analysis of 1000 brains (Yeo et al. 2011) and were projected onto the cortical surface of each individual participant. (B) A ROI analysis was performed on each ROI within the CCN for LTM-guided and STIM-guided conditions. The bar graph presents percent signal change between each condition compared with passive viewing. Error bars reflect SEM. (C and E) Zoomed in images of the medial and lateral left (top) and right (bottom) cortical surfaces during the STIM-guided condition (vs. passive viewing). (D and F) The same views for the LTM-guided (vs. passive viewing). CCN ROIs are outlined in black, DMN ROIs are outlined in white, and DAN ROIs are outlined in green. Black arrows indicate differences between the STIM-guided condition activation and the LTM-guided condition activation. **$P < 0.01$, and ***$P < 0.0001$, Holm–Bonferroni corrected.

(Figs 4A–C and 5). A repeated-measures Hemisphere × ROI × Condition ANOVA was performed, and all statistics are lower-bound corrected (Mauchly's test for sphericity was not met for any of the main effects or interactions; $P < 0.001$). In contrast to the CCN, the DAN showed significantly greater activation in the STIM-guided condition compared with the LTM-guided condition, revealed by a main effect of Condition ($F_{1,22} = 35.93$, $P < 0.001$). There was also a main effect of ROI, but no main effect of Hemisphere ($F_{1,22} = 6.51$, $P = 0.018$ and $F_{1,22} = 3.11$, $P = 0.09$, respectively). All 3 two-way interactions emerged as significant (ROI × Condition: $F_{1,22} = 11.54$, $P = 0.003$; ROI × Hemisphere: $F_{1,22} = 14.47$, $P = 0.001$; and Hemisphere × Condition: $F_{1,22} = 10.62$, $P = 0.004$). The three-way interaction was also significant ($F_{1,22} = 4.65$, $P = 0.042$). Therefore, all post hoc t-tests were performed separately for each hemisphere ROI and Holm–Bonferroni corrected for 34 ROIs. All subdivisions of the DAN were significantly more activated by the STIM-guided than by the LTM-guided attention conditions (all $P < 0.02$ corrected, post hoc paired t-tests; Table 2). The

Hemisphere × Condition interaction reflected a stronger difference between STIM-guided and LTM-guided activation in the RH compared with the left. The ROI × Hemisphere interaction was driven by significantly greater activation of the iPCS in the RH compared with the LH (iPCS: $t_{(22)} = 3.77$, $P = 0.001$; IPS/SPL/LOC: $P = 0.11$; sPCS: $P = 0.42$). Thus, the STIM-guided attention condition more strongly taxed the DAN than did the LTM-guided attention condition, even though no significant behavioral differences were observed.

Default Mode Network and Hippocampus

In contrast to the DAN and CCN, there was no main effect of Condition in the DMN ($F_{1,22} = 3.34$, $P = 0.081$). Also, many nodes of the DMN were deactivated compared with passive viewing (Fig. 4D–F). The results within this network are more complex and heterogeneous than in the other 2 networks. The repeated-measures ANOVA revealed a main effect of ROI ($F_{1,22} = 13.60$,

Table 2 Percent signal change in ROI analysis results for the CCN, DAN, and DMN, defined from the Yeo 7-network parcellation

Region of interest	Hemisphere	LTM-guided	STIM-guided	t-value	P-value
Cognitive control network					
PrC-p	L	0.28 ± 0.05	0.13 ± 0.05	5.04	0.0012
PrC-p	R	0.30 ± 0.04	0.13 ± 0.04	6.84	<0.0001
CaS-p	L	0.20 ± 0.04	0.14 ± 0.03	5.98	0.0001
CaS-p	R	0.24 ± 0.03	0.17 ± 0.03	4.46	0.0043
latIPS	L	0.16 ± 0.04	0.12 ± 0.04	1.62	1.00
latIPS	R	0.17 ± 0.05	0.13 ± 0.04	1.79	1.00
LTC-p	L	0.02 ± 0.06	0.08 ± 0.06	2.06	0.725
LTC-p	R	0.08 ± 0.04	0.09 ± 0.04	0.55	1.00
dmPFC-p	L	0.06 ± 0.03	0.05 ± 0.03	0.57	1.00
dmPFC-p	R	0.11 ± 0.03	0.08 ± 0.03	1.39	1.00
dlPFC	L	0.04 ± 0.03	0.02 ± 0.03	0.838	1.00
dlPFC	R	0.07 ± 0.03	0.05 ± 0.03	0.814	1.00
vlPFC-p	L	0.17 ± 0.04	0.18 ± 0.04	0.218	1.00
vlPFC-p	R	0.19 ± 0.05	0.20 ± 0.04	0.777	1.00
Dorsal attention network					
IPS/SPL	L	0.24 ± 0.04	0.37 ± 0.04	6.54	<0.0001
IPS/SPL	R	0.22 ± 0.04	0.36 ± 0.04	6.81	<0.0001
iPCS	L	0.18 ± 0.04	0.31 ± 0.04	4.51	0.0029
iPCS	R	0.25 ± 0.05	0.43 ± 0.05	6.12	<0.0001
sPCS	L	0.20 ± 0.04	0.26 ± 0.04	3.83	0.0144
sPCS	R	0.18 ± 0.04	0.27 ± 0.04	4.77	0.0016
Default mode network					
PHC	L	0.04 ± 0.03	0.17 ± 0.04	6.92	<0.0001
PHC	R	0.07 ± 0.04	0.25 ± 0.04	7.34	<0.0001
Hippo.	L	0.007 ± 0.02	0.067 ± 0.03	3.53	0.0265
Hippo.	R	−0.004 ± 0.03	0.091 ± 0.02	6.35	<0.0001
PCC	L	0.01 ± 0.03	−0.04 ± 0.03	4.80	0.0021
PCC	R	0.06 ± 0.03	0.02 ± 0.03	3.61	0.0308
dmPFC-a	L	−0.09 ± 0.03	−0.11 ± 0.03	2.41	0.2729
dmPFC-a	R	−0.07 ± 0.03	−0.09 ± 0.03	2.11	0.4647
vlPFC-a	L	−0.10 ± 0.04	−0.06 ± 0.03	2.62	0.1863
vlPFC-a	R	−0.06 ± 0.03	−0.01 ± 0.03	2.81	0.1329
AnG	L	−0.06 ± 0.04	−0.07 ± 0.04	1.06	0.6712
AnG	R	−0.06 ± 0.03	−0.03 ± 0.03	1.92	0.6096
LTC-a	L	−0.02 ± 0.03	−0.02 ± 0.03	0.68	1.0
LTC-a	R	−0.04 ± 0.02	−0.03 ± 0.03	0.58	1.0

Note: All significant values are Holm–Bonferroni corrected for 34 comparisons (total number of ROIs).

$P = 0.001$) and no main effect of Hemisphere in the DMN ($F_{1,22} = 3.50$, $P = 0.075$). Neither of the two-way interactions involving Hemisphere were significant (ROI × Hemisphere: $F_{1,22} = 1.24$, $P = 0.278$; Hemisphere × Condition interaction: $F_{1,22} = 3.85$, $P = 0.063$). However, there was a significant three-way interaction (Hemisphere × ROI × Condition, $F_{1,22} = 5.20$, $P = 0.033$). Therefore, post hoc t-tests were performed separately for each hemisphere for each ROI and Holm–Bonferroni corrected for 34 total ROIs. The heterogeneity of results is indicated by the significant ROI × Condition interaction ($F_{1,22} = 18.79$, $P < 0.001$). The 2 medial temporal lobe structures, PHC and HC, showed greater activation in the STIM-guided condition compared with the LTM-guided condition (all $P < 0.001$, corrected; Table 2). The medial temporal lobe activation in the STIM-guided condition may reflect encoding processes; in each STIM-guided trial, the location of a potential change in an image is shown for the first time and it is likely that participants are encoding this information, while participants have already learned the change locations for LTM-guided trial images.

Bilateral PCC showed greater activation in the LTM-guided than STIM-guided condition (both $P < 0.01$, corrected; Table 2). However, LTM-guided attention did not drive significant positive activation relative to baseline in any of these ROIs, suggesting that the difference in the LTM-guided versus STIM-guided contrast results from deactivation during the STIM-guided condition. A possible explanation is that suppressive influences from the DAN, which is more activated in the STIM-guided condition than the LTM-guided condition, may differentially suppress these medial nodes of the DMN during the STIM-guided condition. No other regions within the DMN showed significant activation differences between the LTM-guided and STIM-guided conditions.

Network ROI Analysis II—Alternative Network Definitions

The ROI analysis above employed a network parcellation based on intrinsic functional connectivity analysis. The 3 subnetworks of the Yeo et al. 7-Network parcellation were an a priori choice for ROI analysis. However, 2 other prominent cortical network parcellations have been reported that are also derived from intrinsic functional connectivity analysis: the Power parcellation (Power et al. 2011) and the Yeo 17-Network parcellation (Yeo et al. 2011). At the suggestion of an anonymous reviewer, we
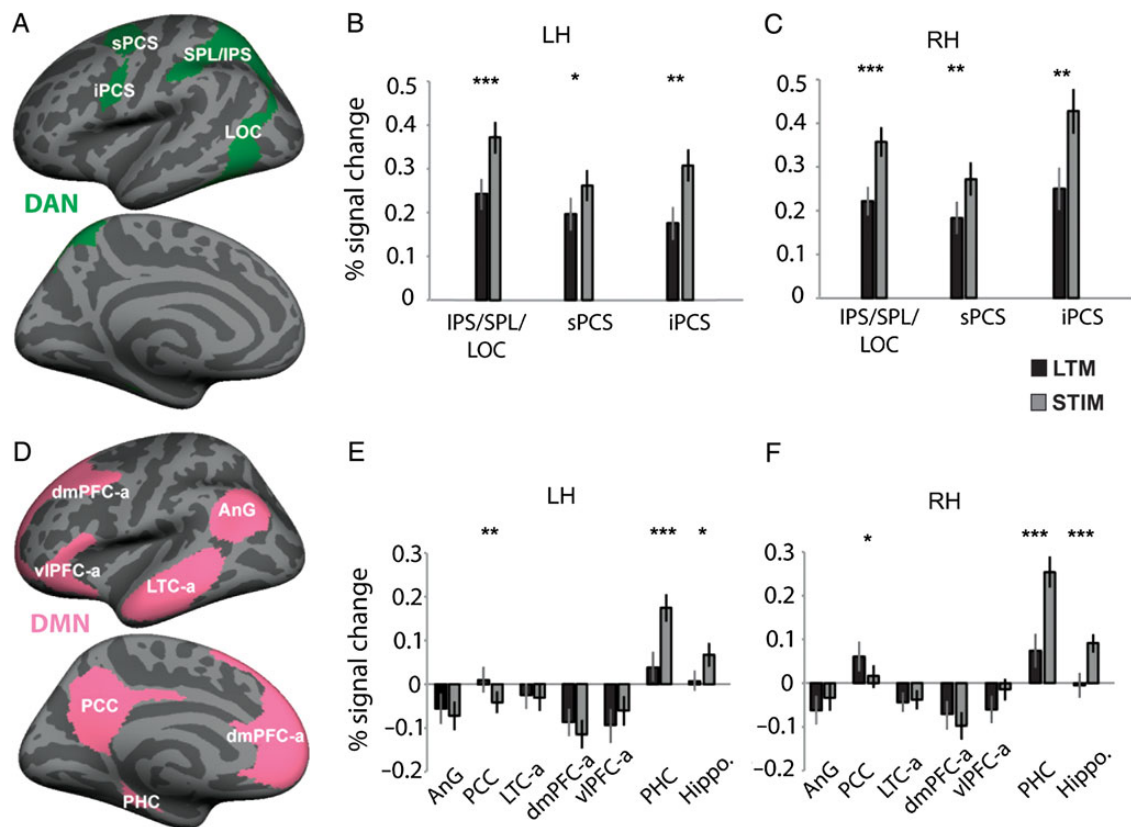
Figure 4. ROI analyses for the *dorsal attention* and default mode networks (DAN and DMN): (A and B) ROIs were obtained from an intrinsic functional connectivity analysis of 1000 brains (Yeo et al. 2011) and were projected onto the cortical surface of each individual participant. ROIs from the DAN and DMN are presented. (C–F) Bar graphs illustrate percent signal change in the LTM-guided and STIM-guided conditions compared with passive viewing for each ROI within the DAN and DMN. *P < 0.05, **P < 0.01, and ***P < 0.0001, Holm–Bonferroni corrected. Error bars reflect SEM.
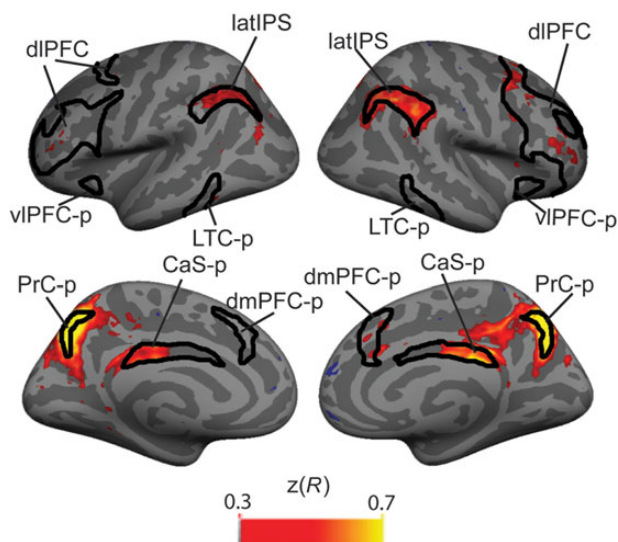

Figure 5. PrC-p seed-based intrinsic connectivity analysis: Black lines outline the CCN. Time courses from each vertex in the brain were correlated with the time course of the PrC-p. Hot colored regions reflect vertices whose time courses were positively correlated with the PrC-p (Fisher's z-transformed R-value).

performed a post hoc analysis of our results using ROIs from the Power and Yeo 17 parcellations, in order to better isolate the pattern of activation seen in the contrast of LTM-guided attention versus STIM-guided attention. Both resting-state parcellations reveal a subnetwork on the medial surface that appears

remarkably similar to the CaS-p and PrC-p ROIs activated in the LTM-guided attention task (Supplementary Fig. 1). To attempt to identify a possible function for this previously undescribed network, Power et al. performed a meta-analysis of task data that suggested that this subnetwork might perform memory retrieval functions (Power et al. 2011). Notably, this analysis also suggested that a small ROI in the latIPS, previously identified in Nelson et al. (2010), was also part of this network and we have included this region in our post hoc analysis. From Yeo and colleagues, we used subregions reported in the 17-network parcellation that correspond to this network in the latIPS, PrC-p, and CaS-p (see Materials and Methods). All 3 of the regions, including latIPS, PrC-p, and CaS-p, showed significantly greater activation during the LTM-guided condition compared with the STIM-guided condition (all P < 0.001 Holm–Bonferroni corrected, Table 3 and Supplementary Fig. 1). This was true for both the Yeo 17-network and Power/Nelson parcellations (Nelson et al. 2010; Power et al. 2011; Yeo et al. 2011). Thus, the Yeo 17-network and the Power/Nelson parcellations more precisely captured the pattern of activation that we observed in our memory-guided attention task than did the Yeo 7-network parcellation. Although post hoc analyses, these ROIs capture the observed pattern of activation remarkably well (Supplementary Fig. 1).

Intrinsic Connectivity Analysis

We examined the intrinsic connectivity within the CCN, focusing on the 3 posterior nodes of the CCN recruited for LTM-guided attention. During rest, PrC-p is strongly correlated within each

Table 3 Post hoc analysis using alternative network ROIs

ROI	x, y, z	Hemisphere	LTM-guided	STIM-guided	t-value	P-value
Yeo et al. (2011, 17 network)						
PrC-p		L	0.22 ± 0.04	0.13 ± 0.03	4.21	0.001
PrC-p		R	0.23 ± 0.04	0.14 ± 0.03	4.48	0.0009
CaS-p		L	0.25 ± 0.04	0.17 ± 0.03	6.04	<0.0001
CaS-p		R	0.25 ± 0.02	0.17 ± 0.03	5.49	0.0001
latIPS		L	0.09 ± 0.04	−0.003 ± 0.04	4.16	0.0014
latIPS		R	0.11 ± 0.05	0.005 ± 0.04	4.80	0.0005
Power et al. (2011)						
PrC-p	−7, −71, 42	L	0.30 ± 0.06	0.10 ± 0.06	5.86	<0.0001
PrC-p	11, −66, 42	R	0.25 ± 0.04	0.08 ± 0.04	6.45	<0.0001
CaS-p	−2, −35, 31	L	0.11 ± 0.05	0.02 ± 0.03	5.28	0.0002
CaS-p	2, −24, 30	R	0.10 ± 0.02	0.07 ± 0.01	4.19	0.0014
Nelson et al. (2010)						
latIPS	40, −62, 48	L	0.07 ± 0.05	−0.07 ± 0.05	4.78	0.0005
latIPS	44, −56, 41	R	0.20 ± 0.06	0.10 ± 0.05	3.11	0.0051

Note: Upon suggestion from an anonymous reviewer, ROI analysis was performed using network definitions from Yeo et al. 17-network parcellation and Power et al. All significant values are Holm–Bonferroni corrected.

hemisphere with the other 2 regions recruited in LTM-guided attention, the latIPS and CaS-p (Fig. 5 and Table 4), with less extensive connectivity to the other nodes of the CCN. CaS-p is strongly correlated with PrC-p and moderately correlated with latIPS, but largely uncorrelated with the rest of the CCN (Supplementary Fig. 2A and Table 4). LatIPS shows strong connectivity with almost the entire CCN at rest, aside from moderate connectivity with the CaS-p (Supplementary Fig. 2B and Table 4). Taken together, these findings suggest that these 3 regions may form a subnetwork at rest in which PrC-p serves as a local hub and latIPS connects this subnetwork to the rest of the CCN.

Discussion

Memory-guided attention is key to our high level of visual performance in familiar environments, serving to efficiently direct our limited attentional resources. The present fMRI experiments investigated cortical networks serving memory-guided attention (Hutchinson and Turk-Browne 2012), contrasting LTM-guided attention with stimulus-guided attention and a baseline condition, using a change detection paradigm. We hypothesized that the CCN would be differentially recruited for LTM-guided attention, and our results support this hypothesis. Closer investigation demonstrates that, within the broader CCN, a posterior subnetwork exists and it is preferentially recruited for LTM-guided attention. This subnetwork consists of a region of latIPS, and 2 medial structures, PrC-p and CaS-p/mid-cingulate. Lateral parietal structures, especially on the LH, have been strongly suggested in prior studies to play an important memory retrieval role (e.g., Wagner et al. 2005; Ciaramelli et al. 2008; Vilberg and Rugg 2008; Hutchinson et al. 2009, 2014; Sestieri et al. 2010; Guerin et al. 2012). In contrast, the 2 medial structures have received limited attention in the literature (Power et al. 2011, 2014; Nelson et al. 2013). Our definition of the CCN derives from analysis of a 1000-brain database (Yeo et al. 2011) and is similar to prior functional connectivity reports (Dosenbach et al. 2007; Vincent et al. 2008); however, we note that some task-based definitions of the CCN differ by including much of the DAN and excluding posterior regions that are the focus of our results (e.g., Cole and Schneider 2007; Braver 2012).

We also examined 2 other networks, that is, the DAN and the DMN. While the DAN was significantly activated in both LTM-guided and STIM-guided conditions, it was more strongly activated for the STIM-guided condition. Since there were no behavioral differences, this activation cannot be attributed to task difficulty, per se; however, the BOLD activation difference suggests that LTM-guided attention was less taxing on the DAN than was STIM-guided attention. Although it is not inconceivable that the greater DAN activation could result from the presence of the explicit spatial cue in the STIM-guided condition, this explanation seems unlikely given that early visual cortex does not exhibit corresponding robust increases in activation for the STIM-guided condition. Thus, the suggestion that LTM-guided attention reduces demands on the DAN deserves further investigation.

We did not observe a main effect for the DMN and no coherent pattern emerges across the ROIs of the DMN. One notable prior study (Summerfield et al. 2006) observed greater LTM-guided attention activation than stimulus-guided attention activation within the left HC, while here the HC was significantly more activated by the STIM-guided condition. Recent work also demonstrated hippocampal activation during the cueing phase of LTM-guided attention (Stokes et al. 2012). In our change detection paradigm, the STIM-guided trials likely activated memory *encoding* mechanisms; any time a change occurred in a STIM-guided trial, it was the first time participants saw a change in that image and it is likely that participants encoded this location into LTM. Previous research has demonstrated that memory encoding robustly activates the HC (e.g., Stern et al. 1996; Wagner et al. 1998). We do not take the present results to contradict the hippocampal involvement in LTM-guided attention in previous studies. We note that, in the present study, stimuli and stimuli changes in the LTM-guided condition were well learned (see Behavioral Results) while in learning may have still been occurring over the course of scanning in Summerfield et al. (2006). This activation in the HC in previous studies may reflect the critical role that the HC plays in binding of relational information (Ryan et al. 2000; Yee et al. 2014). We believe that, in the current study, the LTM-guided condition does not rely on the HC because the stimuli and changes were well learned. In contrast, the additional

Table 4 Intrinsic connectivity using PrC-p (left: −9.5 −67.3, 42.8; right: 10.1, −65.9, 41.2), CaS-p (left: −6.0, −23.1, 29.3; right: 6.6, −17.9, 29.8), and latIPS (left: −36.5, −56.2, 38.2; right: 37.5, −57.3, 40.5) as seed regions within the hemisphere

Anatomical region	x	y	z	Size (mm^2)	t-value
Left PrC-p seed					
PrC-p (CCN)	−9.0	−69.8	46.3	4326.51	8.630
CaS-p (CCN)	−8.4	−36.8	25.3	645.53	5.285
dlPFC (CCN)	−40.8	28.5	21.9	879.40	4.490
latIPS (CCN)	−39.9	−60.1	41.7	1956.53	4.485
LTC-p (CCN)	−53.6	−55.0	−16.9	196.23	4.121
Occipital pole (visual)	−11.4	−96.6	−10.8	433.47	3.436
IPS (DAN)	−41.6	−76.8	15.6	286.14	3.324
Right PrC-p seed					
PrC-p (CCN)	8.7	−67.3	40.5	3522.27	8.830
CaS-p (CCN)	6.5	−30.6	29.0	781.59	6.690
latIPS (CCN)	42.1	−70.2	35.4	3655.26	5.445
dmPFC-p (CCN)	13.6	23.9	28.5	204.94	4.712
dlPFC (CCN)	45.7	29.8	22.9	1724.41	4.680
	39.3	51.3	8.0	264.14	3.229
dmPFC-p (CCN)	7.6	19.3	46.8	204.72	3.878
Insula (VAN)	30.5	19.4	9.0	201.66	3.430
Left CaS-p seed					
CaS-p (CCN/DMN)	−5.2	−34.7	29.1	1421.10	11.708
	−8.3	22.8	27.1	515.48	4.786
PrC-p (CCN)	−15.3	−70.8	36.4	1184.83	6.660
latIPS/TPJ (DAN/VAN)	−53.8	−42.6	45.5	242.23	4.934
Insula (VAN)	−34.6	14.5	−3.5	469.08	5.292
	−35.8	39.4	10.5	164.47	2.653
Right CaS-p seed					
CaS-p (CCN)	5.8	−28.7	30.5	2217.54	10.446
PrC-p (CCN)	14.2	−69.1	38.9	955.38	5.631
latIPS (CCN)	52.6	−45.3	37.8	1123.63	5.051
	35.5	−69.7	42.7	211.65	4.152
vlPFC-p (CCN/VAN)	31.6	15.0	−8.3	511.28	3.129
Left latIPS seed					
latIPS (CCN/DAN)	−40.7	−45.9	36.6	3582.97	9.621
PrC-p (CCN)	−5.9	−65.2	43.5	831.41	4.550
dlPFC/iPCS (CCN/DAN)	−42.9	1.8	24.9	4672.24	7.305
LTC-p/LOC (CCN/DAN)	−47.6	−56.9	−8.7	1790.88	5.019
dmPFC-p (CCN)	−6.7	26.3	41.4	351.82	5.008
Occipital pole (visual)	−19.3	−100.9	−4.7	226.64	3.134
LOC (visual)	−36.2	−88.0	−11.1	318.03	2.619
Right latIPS seed					
latIPS (CCN)	34.4	−58.1	44.2	3446.39	9.659
PrC-p (CCN)	6.6	−61.5	41.1	1099.37	5.533
dlPFC(CCN)	28.3	6.8	48.6	6695.62	7.054
dmPFC-p (CCN)	8.5	29.4	40.9	395.19	6.707
CaS-P (CCN)	5.8	−38.9	24.0	1002.28	5.708
Insula (VAN)	32.7	18.9	2.1	205.87	5.263
LTC-p (CCN)	62.4	−38.5	−13.5	1471.81	5.093

Note: Seeds were defined as vertices within the CCN network definition that were significantly (P < 0.01) recruited for LTM-guided attention versus baseline.

encoding of the changes in the STIM-guided scenes resulted in overall more activation in the HC for the STIM-guided scenes than the LTM-guided scenes.

Previous work has shown that the activity within the CCN is positively correlated with both the DMN and DAN at rest (Spreng et al. 2013), suggesting that these regions may be well positioned

to act as an intermediary between regions of the DMN and DAN. Here, we sought to characterize the specific intrinsic connectivity profile of each of the regions within the CCN recruited for LTM-guided attention. No prior studies have described the connectivity patterns between all 3 of these nodes. When the PrC-p was used as a seed for resting-state functional connectivity, we found strong positive correlations with CaS-p and latIPS, but less extensive connectivity with the other nodes of the CCN (Fig. 5 and Table 4). CaS-p exhibited strong resting-state functional connectivity only with PrC-p and itself (Supplementary Fig. 2A and Table 4); this observation is consistent with prior reports that CaS-p and PrC-p form a distinct two-node resting-state network (Power et al. 2011, 2014; Yeo et al. 2011). In contrast, latIPS exhibits strong resting-state functional connectivity throughout the broader CCN (Supplementary Fig. 2B). Therefore, we suggest that PrC-p serves as a local hub in this three-node memory-guided attention network, and that latIPS serves as hub to the broader CCN. Thus, our analysis illuminates a subnetwork of the CCN and its potential role in memory-guided attention. A recent fMRI study (Nelson et al. 2013) noted that these 3 regions may contribute in a broader range of memory retrieval operations. The full functional range of this network deserves further investigation.

Involvement of CaS-p, PrC-p, and latIPS was not reported in the 2 prior studies employed fMRI to investigate memory-guided attention (e.g., Summerfield et al. 2006; Stokes et al. 2012). The present study likely benefitted from the use of predefined cortical surface ROIs, as some CCN regions lie between DMN and DAN regions and could be obscured by volume-based group-averaging methods. Of these, prior studies only one study directly contrasted memory-guided attention with exogenous stimulus-guided attention (Summerfield et al. 2006); the present findings differ significantly, but there are some important similarities. Summerfield et al. (2006) observed that both memory-guided attention and exogenous stimulus-guided attention drove a common network of brain regions including the mid-cingulate as well as multiple regions of the fronto-parietal DAN. Here, we confirm that the mid-cingulate and the DAN were activated in both conditions, but we also observed significant activation differences between conditions. The mid-cingulate cortex exhibited greater activation for LTM-guided attention, whereas the DAN exhibited greater activation for STIM-guided attention.

This study provides the first evidence that 3 regions within the broader CCN are preferentially recruited for memory-guided attention and the first to explicitly investigate the connectivity profiles of each of these nodes. While one recent study (Nelson et al. 2013) has identified these 3 regions in a memory retrieval experiment, our work makes a novel and substantial contribution to understanding these regions as a subnetwork and their function in supporting memory-guided attention.

The PrC-p ROI within the CCN is thin and crescent-shaped, and thus could be easily obscured in volume-based group-averaging techniques. Despite this unusual shape, memory-guided attention activation falls neatly within the boundaries of this ROI (Fig. 3D). A similarly located region, referred to as the medial SPL, has been implicated in an array of task-switching paradigms (Chiu and Yantis 2009; Esterman et al. 2009). In the current task, participants switch attention between their internal representation of the scene change and the external scene. Here, the PrC-p could be participating in this switching between internally directed to externally directed attention. Retrieval of episodic memories also produces activation in this vicinity (Sestieri et al. 2010). Taken together, the data suggest that this region is well positioned to aid in the cooperation of LTM and attention systems.

The CaS-p within the CCN is a long, thin region that may also be described as the rostro-ventral portion of posterior cingulate cortex (Brodmann area 23) or simply as mid-cingulate cortex. Anatomical studies in monkeys and connectivity studies in humans reveal that both the HC and posterior parietal cortex make substantial connections with the mid-cingulate cortex (Baleydier and Mauguière 1987; Vogt et al. 2006; Beckmann et al. 2009). The anatomy suggests that this region is well positioned to support the interaction between memory retrieval and attention. Prior functional connectivity and task activation studies suggest that posterior cingulate cortex consists of several functionally distinct subregions (Vogt et al. 2006; Beckmann et al. 2009; Leech et al. 2011). Prior task-based fMRI studies have reported CaS-p/mid-cingulate activation during retrieval of visual LTM (Huijbers et al. 2011) and retrieval of visual working memory (Schon et al. 2009). Reduced CaS-p/mid-cingulate activation has been observed in clinical populations during cognitive control tasks such as task-switching and N-back working memory tasks (Tamm et al. 2004; Gundersen et al. 2008). Generally, CaS-p/mid-cingulate has been understudied and underemphasized; future studies will be required to more fully explore the functional roles of CaS-p. Our task-based findings demonstrate a strong role for this region in LTM guidance of attention.

A bilateral region in latIPS/AnG was significant in our whole-cortex cluster analysis, did not emerge as significant in the planned Yeo 7-Network ROI analysis, and was highly significant in the post hoc analysis suggested by a reviewer. We interpret these results to indicate that there is a region of latIPS contributed to LTM-guided visual attention, but that this region was not well captured by the Yeo 7-Network parcellation. Our latIPS/AnG activation peak is located near regions previously identified in neuroimaging studies examining the role of parietal cortex in episodic memory retrieval (Wagner et al. 2005; Ciaramelli et al. 2008; Vilberg and Rugg 2008; Hutchinson et al. 2009, 2014; Sestieri et al. 2010). The MNI coordinates for the left latIPS/AnG in our LTM-guided > STIM-guided contrast (−48.6, −58.9, 38.2) lie within 3.5 mm of the average of the locations identified in 2 meta-analyses of left parietal lobe involvement in episodic memory retrieval for recollection (Vilberg and Rugg 2008: −43, −66, 38) and bottom-up attentional capture by retrieved memory contents (Ciaramelli et al. 2008: −50, −57, 38). A peak shift effect (between LTM-guided vs. STIM-guided and LTM-guided vs. passive) that we observed here may help to explain anatomical variability in the location of episodic memory retrieval-based activation in the lateral parietal cortex reported across prior studies [see also Hutchinson et al. (2014)]; the degree of DMN deactivation in the control condition determines the size of the shift. Our latIPS region appears to roughly correspond to a latIPS region sensitive to source memory that may act as a mnemonic accumulator and in the service of memory-guided action selection (Hutchinson et al. 2014). Other studies have also suggested that a region in this vicinity may act in "post-retrieval" processes (Nelson et al. 2010; Sestieri et al. 2011). In the present study, the latIPS may be holding spatial information that has already been retrieved and/or accumulating information about whether a stimulus matches what is stored in memory at that location and thus be acting as a memory-guided action selector. Another recent study has implicated this region in violations of an expected memory response (i.e., unexpected familiarity or unexpected novelty), suggesting that this region may reflect general orienting mechanisms during memory retrieval (Jaeger et al. 2013).

Memory consists of multiple systems, and it follows that memory-guided attention is likely not a single entity [see also Jiang et al. (2013)]. Here, we have focused on the mechanisms by which explicit memory guides visuospatial attention. Retrieval of explicit memories to guide attention may be critical to CCN recruitment, and CCN recruitment may not occur in implicit memory-guided attention paradigms such as contextual cueing (Chun and Jiang 1998; Chun 2000). The spatial nature of the attentional task may have biased CCN activation toward the posterior nodes, as spatial processing is often associated with the posterior cortex (e.g., Posner et al. 1984; Postle et al. 2000); alternately, this may reflect episodic memory influences on reactive cognitive control mechanisms (Braver 2012). In the present study, functional connectivity results and task activations demonstrate functional heterogeneity within the CCN [see also Cole and Schneider (2007)], and point to memory-guided attention as one key function of some CCN nodes.

Traditionally, attention and LTM have been distinct fields of study, examined by different sets of researchers focused on different brain structures. Recent work examining the role of parietal cortex in episodic memory retrieval (Wagner et al. 2005; Ciaramelli et al. 2008, 2010; Vilberg and Rugg 2008; Hutchinson et al. 2009, 2014; Nelson et al. 2010; Sestieri et al. 2010, 2011) and work investigating LTM influences on attention (Chun and Jiang 1998, 2003; Henderson and Hollingworth 1999; Moores et al. 2003; Hollingworth 2004, 2005; Summerfield et al. 2006, 2011; Chun and Turk-Browne 2007; Olivers 2011; Stokes et al. 2012) have started to break through this divide. The present study makes a significant contribution to the field by highlighting the role that this posterior subnetwork within the greater CCN plays in aiding cooperative interactions between memory and attention.

Supplementary Material

Supplementary material can be found at: http://www.cercor.oxfordjournals.org/.

Funding

Notes

The authors thank Karin Schon for providing scene stimuli and Lingqiang Kong for help with data collection and programming assistance. *Conflict of Interest*: None declared.

References

Awh E, Pashler H. 2000. Evidence for split attentional foci. J Exp Psychol Hum Percept Perform. 26:834–846.

Baleydier C, Mauguière F. 1987. Network organization of the connectivity between parietal area 7, posterior cingulate cortex and medial pulvinar nucleus: a double fluorescent tracer study in monkey. Exp Brain Res. 66:385–393.

Beckmann M, Johansen-Berg H, Rushworth MFS. 2009. Connectivity-based parcellation of human cingulate cortex and its relation to functional specialization. J Neurosci. 29:1175–1190.

Braver TS. 2012. The variable nature of cognitive control: a dual mechanisms framework. Trends Cogn Sci. 16:106–113.

Buckner RL, Andrews-Hanna JR, Schacter DL. 2008. The brain's default network: anatomy, function, and relevance to disease. Ann N Y Acad Sci. 1124:1–1138.

Buckner RL, Vincent JL. 2007. Unrest at rest: default activity and spontaneous network correlations. NeuroImage. 37:1091–1099.

Cabeza R. 2008. Role of parietal regions in episodic memory retrieval: the dual attentional processes hypothesis. Neuropsychologia. 46:1813–1827.

Carp J. 2013. Optimizing the order of operations for movement scrubbing: Comment on Power et al. NeuroImage. 76:436–438.

Cave KR, Bush WS, Taylor TGG. 2010. Split attention as part of a flexible attentional system for complex scenes: comment on Jans, Peters, and De Weerd. Psychol Rev. 117:685–696.

Chiu YC, Yantis S. 2009. A domain-independent source of cognitive control for task sets: shifting spatial attention and switching categorization rules. J Neurosci. 29:3930–3938.

Chun MM. 2000. Contextual cueing of visual attention. Trends Cogn Sci. 4:170–178.

Chun M, Jiang Y. 2003. Implicit, long-term spatial contextual memory. J Exp Psychol Learn Mem Cogn. 29:224–234.

Chun MM, Jiang Y. 1998. Contextual cueing: implicit learning and memory of visual context guides spatial attention. Cogn Psychol. 36:28–71.

Chun MM, Turk-Browne NB. 2007. Interactions between attention and memory. Curr Opin Neurobiol. 17:177–184.

Ciaramelli E, Grady CL, Levine B, Ween J, Moscovitch M. 2010. Top-down and bottom-up attention to memory are dissociated in posterior parietal cortex: neuroimaging and and neuropsychological evidence. J Neurosci. 30:4943–4956.

Ciaramelli E, Grady CL, Moscovitch M. 2008. Top-down and bottom-up attention to memory: a hypothesis (AtoM) on the role of the posterior parietal cortex in memory retrieval. Neuropsychologia. 46:1828–1851.

Cole MW, Schneider W. 2007. The cognitive control network: Integrated cortical regions with dissociable functions. NeuroImage. 37:343–360.

Corbetta M, Shulman GL. 2002. Control of goal-directed and stimulus-driven attention in the brain. Nat Rev Neurosci. 3:201–215.

Cowan N. 2001. The magical number 4 in short-term memory: a reconsideration of mental storage capacity. Behav Brain Sci. 24:87–114. discussion 114–185.

Dale AM, Fischl B, Sereno MI. 1999. Cortical surface-based analysis. I. Segmentation and surface reconstruction. NeuroImage. 9:179–194.

Dosenbach NUF, Fair DA, Miezin FM, Cohen AL, Wenger KK, Dosenbach RA, Fox MD, Snyder AZ, Vincent JL, Raichle ME, et al. 2007. Distinct brain networks for adaptive and stable task control in humans. Proc Natl Acad Sci USA. 104: 11073–11078.

Esterman M, Chiu Y-C, Tamber-Rosenau BJ, Yantis S. 2009. Decoding cognitive control in human parietal cortex. Proc Natl Acad Sci USA. 106:17974–17979.

Fischl B. 2012. FreeSurfer. NeuroImage. 62:774–781.

Fischl B, Salat DH, Busa E, Albert M, Dieterich M, Haselgrove C, van der Kouwe A, Killiany R, Kennedy D, Klaveness S, et al. 2002. Whole brain segmentation: automated labeling of neuroanatomical structures in the human brain. Neuron. 33:341–355.

Fischl B, Sereno MI, Dale AM. 1999. Cortical surface-based analysis. II: inflation, flattening, and a surface-based coordinate system. NeuroImage. 9:195–207.

Fischl B, Sereno MI, Tootell RB, Dale AM. 1999. High-resolution intersubject averaging and a coordinate system for the cortical surface. Hum Brain Mapp. 8:272–284.

Forman SD, Cohen JD, Fitzgerald M, Eddy WF, Mintun MA, Noll DC. 1995. Improved assessment of significant activation in functional magnetic resonance imaging (fMRI): use of a cluster-size threshold. Magn Reson Med. 33:636–647.

Fox MD, Snyder AZ, Vincent JL, Corbetta M, Van Essen DC, Raichle M. 2005. The human brain is intrinsically organized into dynamic, anticorrelated functional networks. Proc Natl Acad Sci USA. 102:9673–9678.

Greicius MD, Supekar K, Menon V, Dougherty RF. 2009. Resting-state functional connectivity reflects structural connectivity in the default mode network. Cereb Cortex. 19:72–78.

Guerin SA, Robbins CA, Gilmore AW, Schacter DL. 2012. Interactions between visual attention and episodic retrieval: dissociable contributions of parietal regions during gist-based false recognition. Neuron. 75:1122–1134.

Gundersen H, Specht K, Grüner R, Ersland L, Hugdahl K. 2008. Separating the effects of alcohol and expectancy on brain activation: an fMRI working memory study. NeuroImage. 42:1587–1596.

Hagler DJ, Sereno MI. 2006. Spatial maps in frontal and prefrontal cortex. NeuroImage. 29:567–577.

Henderson JM, Hollingworth A. 1999. High-level scene perception. Ann Rev Psychol. 50:243–271.

Hollingworth A. 2004. Constructing visual representations of natural scenes: the roles of short- and long-term visual memory. J Exp Psychol Hum Percept Perform. 30:519–537.

Hollingworth A. 2005. The relationship between online visual representation of a scene and long-term scene memory. J Exp Psychol Learn Mem Cogn. 31:396–411.

Huijbers W, Pennartz CMA, Rubin DC, Daselaar SM. 2011. Imagery and retrieval of auditory and visual information: neural correlates of successful and unsuccessful performance. Neuropsychologia. 49:1730–1740.

Hutchinson JB, Turk-Browne NB. 2012. Memory-guided attention: control from multiple memory systems. Trends Cogn Sci. 16:576–579.

Hutchinson JB, Uncapher MR, Wagner AD. 2009. Posterior parietal cortex and episodic retrieval: convergent and divergent effects of attention and memory. Learn Mem. 16: 343–356.

Hutchinson JB, Uncapher MR, Weiner KS, Bressler DW, Silver MA, Preston AR, Wagner AD. 2014. Functional heterogeneity in posterior parietal cortex across attention and episodic memory retrieval. Cereb Cortex. 24:49–66.

Jaeger A, Konkel A, Dobbins IG. 2013. Unexpected novelty and familiarity orienting responses in lateral parietal cortex during recognition judgment. Neuropsychologia. 51:1061–1076.

Jiang YV, Swallow KM, Rosenbaum GM. 2013. Guidance of spatial attention by incidental learning and endogenous cuing. J Exp Psychol Hum Percept Perform. 39:285–297.

Konen CS, Kastner S. 2008. Representation of eye movements and stimulus motion in topographically organized areas of human posterior parietal cortex. J Neurosci. 28:8361–8375.

Leech R, Kamourieh S, Beckmann CF, Sharp DJ. 2011. Fractionating the default mode network: distinct contributions of the ventral and dorsal posterior cingulate cortex to cognitive control. J Neurosci. 31:3217–3224.

McMains SA, Somers DC. 2004. Multiple spotlights of attentional selection in human visual cortex. Neuron. 42:677–686.

McMains SA, Somers DC. 2005. Processing efficiency of divided spatial attention mechanisms in human visual cortex. J Neurosci. 25:9444–9448.

Moores E, Laiti L, Chelazzi L. 2003. Associative knowledge controls deployment of visual selective attention. Nat Neurosci. 6:182–189.

Nelson SM, Arnold KM, Gilmore AW, McDermott KB. 2013. Neural signatures of test-potentiated learning in parietal cortex. J Neurosci. 33(29):11754–11762.

Nelson SM, Cohen AL, Power JD, Wig GS, Miezin FM, Wheeler ME, Velanova K, Donaldson DI, Phillips JS, Schlaggar BL, et al. 2010. A parcellation scheme for human left lateral parietal cortex. Neuron. 67:156–170.

Olivers C. 2011. Long-term visual associations affect attentional guidance. Acta Psychol. 137:243–247.

Patai EZ, Doallo S, Nobre AC. 2012. Long-term memories bias sensitivity and target selection in complex scenes. J Cogn Neurosci. 24:2281–2291.

Posner MI, Walker JA, Friedrich FJ, Rafal RD. 1984. Effects of parietal injury on covert orienting of attention. J Neurosci. 4:1863–1874.

Postle BR, Stern CE, Rosen BR, Corkin S. 2000. An fMRI investigation of cortical contributions to spatial and nonspatial visual working memory. NeuroImage. 11:409–423.

Power JD, Barnes KA, Snyder AZ, Schlaggar BL, Petersen SE. 2012. Spurious but systematic correlations in functional connectivity MRI networks arise from subject motion. NeuroImage. 59:2142–2154.

Power JD, Barnes KA, Snyder AZ, Schlaggar BL, Petersen SE. 2013. Steps toward optimizing motion artifact removal in functional connectivity MRI; a reply to Carp. NeuroImage. 76:439–441.

Power JD, Cohen AL, Nelson SM, Wig GS, Barnes KA, Church JA, Vogel AC, Laumann TO, Miezin FM, Schlaggar BL, et al. 2011. Functional network organization of the human brain. Neuron. 72:665–678.

Power JD, Schlaggar BL, Petersen SE. 2014. Studying brain organization via spontaneous fMRI signal. Neuron. 84:681–696.

Pylyshyn ZW, Storm RW. 1988. Tracking multiple independent targets: evidence for a parallel tracking mechanism. Spat Vis. 3:179–197.

Raichle ME, MacLeod AM, Snyder AZ, Powers WJ, Gusnard DA, Shulman GL. 2001. A default mode of brain function. Proc Natl Acad Sci USA. 98:676–682.

Rensink RA, O'Regan JK, Clark JJ. 1997. To see or not to see: the need for attention to perceive changes in scenes. Psychol Sci. 8:368–373.

Rosen ML, Stern CE, Somers DC. 2014. Long-term memory guidance of visuospatial attention in a change-detection paradigm. Front Psychol. 5:266

Ryan JD, Althoff RA, Whitlow S, Cohen NJ. 2000. Amnesia is a deficit in relational memory. Psychol Sci. 11(6):454–461.

Schon K, Quiroz YT, Hasselmo ME, Stern CE. 2009. Greater working memory load results in greater medial temporal activity at retrieval. Cereb Cortex. 19:2561–2571.

Sestieri C, Corbetta M, Romani GL, Shulman GL. 2011. Episodic memory retrieval, parietal cortex, and the default mode network: functional and topographic analyses. J Neurosci. 31:4407–4420.

Sestieri C, Shulman GL, Corbetta M. 2010. Attention to memory and the environment: functional specialization and dynamic competition in human posterior parietal cortex. J Neurosci. 30:8445–8456.

Shomstein S, Yantis S. 2004. Control of attention shifts between vision and audition in human cortex. J Neurosci. 24:10702–10706.

Shomstein S, Yantis S. 2006. Parietal cortex mediates voluntary control of spatial and nonspatial auditory attention. J Neurosci. 26:435–439.

Simons DJ, Chabris CF. 1999. Gorillas in our midst: sustained inattentional blindness for dynamic events. Perception. 28:1059–1074.

Spreng RN, Sepulcre J, Turner GR, Stevens WD, Schacter DL. 2013. Intrinsic architecture underlying the relations among the default, dorsal attention, and frontoparietal control networks of the human brain. J Cogn Neurosci. 25:74–86.

Stern CE, Corkin S, González RG, Guimaraes AR, Baker JR, Jennings PJ, Carr CA, Sugiura RM, Vedantham V, Rosen BR. 1996. The hippocampal formation participates in novel picture encoding: evidence from functional magnetic resonance imaging. Proc Natl Acad Sci USA. 93:8660–8665.

Stokes MG, Atherton K, Patai EZ, Nobre AC. 2012. Long-term memory prepares neural activity for perception. Proc Natl Acad SciUSA. 109:E360–E367.

Straw AD. 2008. Vision egg: an open-source library for realtime visual stimulus generation. Front Neuroinformatics. 2:4.

Summerfield JJ, Lepsien J, Gitelman DR, Mesulam MM, Nobre AC. 2006. Orienting attention based on long-term memory experience. Neuron. 49:905–916.

Summerfield JJ, Rao A, Garside N, Nobre AC. 2011. Biasing perception by spatial long-term memory. J Neurosci. 31: 14952–14960.

Tamm L, Menon V, Ringel J, Reiss AL. 2004. Event-related FMRI evidence of frontotemporal involvement in aberrant response inhibition and task switching in attention-deficit/hyperactivity disorder. J Am Acad Child Adolesc Psychiatry. 43:1430–14340.

Van Dijk KR, Hedden T, Venkataraman A, Evans KC, Lazar SW, Buckner RL. 2010. Intrinsic functional connectivity as a tool for human connectomics: theory, properties, and optimization. J Neurophysiol. 103:297–321.

Vilberg KL, Rugg MD. 2009. Left parietal cortex is modulated by amount of recollected verbal information. Neuroreport. 20:1295–1299.

Vilberg KL, Rugg MD. 2008. Memory retrieval and the parietal cortex: a review of evidence from a dual-process perspective. Neuropsychologia. 46:1787–1799.

Vincent JL, Kahn I, Snyder AZ, Raichle ME, Buckner RL. 2008. Evidence for a frontoparietal control system revealed by intrinsic functional connectivity. J Neurophysiol. 100:3328–3342.

Vincent JL, Snyder AZ, Fox MD, Shannon BJ, Andrews JR, Raichle ME, Buckner R. 2006. Coherent spontaneous activity identifies a hippocampal-parietal memory network. J Neurophysiol. 96: 3517–3531.

Vogt BA, Vogt L, Laureys S. 2006. Cytology and functionally correlated circuits of human posterior cingulate areas. NeuroImage. 29:452–466.

Wagner AD, Schacter DL, Rotte M, Koutstaal W, Maril A, Dale AM, Rosen BR, Buckner RL. 1998. Building memories: remembering and forgetting of verbal experiences as predicted by brain activity. Science. 281:1188–1891.

Wagner AD, Shannon BJ, Kahn I, Buckner RL. 2005. Parietal lobe contributions to episodic memory retrieval. Trends Cogn Sci. 9:445–453.

Yee LTS, Hannula DE, Tranel D, Cohen NJ. 2014. Short-term retention of relational memory in amnesia revisited: accurate performance depends on hippocampal integrity. Front Hum Neuroci. 8:16.

Yeo BT, Krienen FM, Sepulcre J, Sabuncu MR, Lashkari D, Hollinshead M, Roffman JL, Smoller JW, Zollei L, Polimeni JR, et al. 2011. The organization of the human cerebral cortex estimated by intrinsic functional connectivity. J Neurophysiol. 106:1125–1165.